RESEARCH ARTICLE
doi: 10.2306/scienceasia1513-1874.2026.024

*ScienceAsia* 52 (1): 2026: ID 2026024: **1–7**

# Optimizing the oxidation time of Spiro-OMeTAD hole transport layer for enhanced performance in perovskite solar cells

**Gltad Alas[a], Ya-li Zhu[a], Chen-hua Huang[a], Ru-yi Tang[a], Bao Asina[a], Lin-rui Zhang[a,b], Ying-Jie Li[a,b], Jun Ning[a,b,*], Hexig Alata[a,b,*]**

[a] College of Physics and Electronic Information, Inner Mongolia Normal University, Hohhot 010022 China
[b] Inner Mongolia Key Laboratory for Applied Condensed Matter Physics, Inner Mongolia Normal University, Hohhot 010022 China

*Corresponding authors, e-mail: ningjun@imnu.edu.cn, alata@imnu.edu.cn

*Received 16 Sep 2025, Accepted 25 Feb 2026*
*Available online 22 Mar 2026*

**ABSTRACT**: Perovskite solar cells (PSCs) have great potential to achieve high-efficiency and low-cost photovoltaic devices. 2,2′,7,7′-tetrakis-(N,N-dip-methoxyphenylamine)-9,9′-spirobifluorene (Spiro-OMeTAD) is widely used as a hole transport layer (HTL) in high-performance PSCs. However, Spiro-OMeTAD has poor conductivity. To address this limitation, it is typically doped with hygroscopic additives, such as lithium bistrifluoromethylsulfonamide (Li-TFSI) and 4-tert-butylpyridine (tBP). Unfortunately, its inherent humidity sensitivity limits both performance and stability of PSCs. There are a few systematic investigations into the effect of Spiro-OMeTAD oxidation time on PSC performance. This study systematically investigates the influence of varying oxidation times on the photovoltaic performance in PSCs with Spiro-OMeTAD HTL. We fabricated PSCs with an indium tin oxide (ITO)/tin oxide (ceSnO2)/perovskite/Spiro-OMeTAD/Silver (Ag) architecture. The oxidation time of the Spiro-OMeTAD layer was tuned between 24 and 168 h. It was found that an oxidation time of 96 h was optimum for the crystallization of Spiro-OMeTAD film, thereby minimizing defect density and enhancing carrier transport. This results in a power conversion efficiency (PCE) of 16.80%. The optimal oxidation time effectively suppresses non-radiative recombination and improves the stability of PSC. Our findings underscore the critical role of precise oxidation control in HTLs and provide a straightforward approach to boost PSC performance.

**KEYWORDS**: perovskite solar cells, carrier transport, hole transport layer, oxidation

## INTRODUCTION

Perovskite solar cells (PSCs) have attracted considerable attention [1] because of their numerous advantages, including low cost [2], minimal energy consumption [3], a simple fabrication process [4], and exceptionally high photoelectric conversion efficiencies [5, 6]. Over the past decade, the photoelectric conversion efficiency of PSCs has rapidly increased from 3.8% to 27% [7, 8]. The typical structure of PSCs consists of an electron transport layer [9], a perovskite layer [10], a hole transport layer (HTL), and an electrode [11]. Carrier transport properties are crucial in determining the efficiency of PSCs [12].

The HTL material plays a pivotal role in high-efficiency PSCs. A variety of HTL materials have been reported, including poly[bis(4 phenyl)(2,4,6 trimethylphenyl)amine] (PTAA) [13], poly(3,4 ethylenedioxythiophene) poly(styrenesulfonate) (PEDOT:PSS) [14], HTM-T2 [15], XC2-M, and XC2-H [16]. These materials all exhibit remarkable charge transport capabilities and compatibility with perovskite absorbers. Spiro-OMeTAD is the most widely adopted in both research and applications [17, 18]. However, its low conductivity and carrier mobility [19, 20] lead to low efficiency of PSCs with Spiro-OMeTAD HTL [21]. Currently, the predominant and most effective strategy to address this limitation involves the indirect oxidation of Li-TFSI [22] and tBP [23] using atmospheric oxygen. Oxygen and water serve as oxidants [24], while Spiro-OMeTAD acts as the reductant, and $Li^+$ functions as the supporting ion to complete the electrochemical cycle [25, 26]. Nevertheless, a key challenge arises from the hygroscopic nature of Li-TFSI [27], which makes the Spiro-OMeTAD layer more susceptible to atmospheric moisture during the oxidation process [28]. This hygroscopicity also induces instability in the resulting PSCs under high-humidity conditions, compromising their ability to maintain an optimal photoelectric conversion efficiency [29]. Hence, determining the optimal oxidation time is essential for obtaining high-performance PSCs with Spiro-OMeTAD film as the HTL [30, 31].

In this work, we systematically investigated the effect of varying the oxidation time of Spiro-OMeTAD films employed as the HTLs. By precisely controlling the oxidation time, we clarified its impact on both PSC performance and carrier transport properties. Our findings not only advance the understanding of the underlying mechanisms but also provide valuable insights for optimizing the design and performance of PSCs.

## MATERIALS AND METHODS

Materials for the experiment: $SnO_2$ aqueous solution from Alfa Aesar (Shanghai, China) was selected as the precursor solution; isopropanol (IPA), dimethyl sulfoxide (DMSO), chlorobenzene (CB) N,N-dimethylformamide (DMF) were purchased from Acros (Beijing, China); Formamidinium Iodide (FAI), methyl bromide (MABr) and methyl chloride (MACl) were purchased from Greatcell solar materials (Sydney, Australia); PbI2 was purchased from TCI (Shanghai, China); the indium tin oxide (ITO) conductive glass was purchased from South China Chemical Technology Co., Ltd. (Shenzhen, China).

PSCs Fabrication: The ITO conductive glass was cleaned with deionized water, acetone, detergent, deionized water, and IPA in turn. Before use, the ITO substrate was cleaned with ozone for 20 min. Then, $SnO_2$ aqueous solution (2.67%) was spin-coated on the ITO substrate at 4,000 rpm for 30 s in indoor ambient air, and annealed on a hot plate at 150 °C for 30 min. To fabricate perovskite films, two step-method was used. First, a 1.4 M concentration of $PbI_2$ (DMF:DMSO = 9.5:0.5) was spin-coated at 1500 rpm for 30 s, and then annealed at 70 °C for 1 min. Second, a mixed solution of FAI:MABr:MACl (60 mg:6 mg:6 mg/1 ml IPA) was spin-coated onto PbI2 film at 1,000 rpm for 30 s. The prepared perovskite film was immediately annealed in the glove box at 70 °C for 1 min, and then transferred to indoor air environment (30–40% humidity) following post-annealing at 150 °C for 20 min. The Spiro-OMeTAD solution was spin-coated at 3000 rpm for 30 s on the perovskite layer. The solution was composed of 72.3 mg Spiro-OMeTAD, 35 µl Li-TFSI solution (260 mg Li-TFSI dissolved in 1 ml acetonitrile), 30 µl tBP, and 1 ml chlorobenzene. The oxidation reaction proceeded under anhydrous conditions within a temperature range of 20–25 °C. Finally, the 100 nm Ag film was thermally evaporated through a shadow mask in a vacuum chamber.

Device testing and characterization: The J-V curve test was performed on the device under the illumination of AM1.5G using Keithley 2400 digital original table and standard solar light source (the light intensity is 100 mW/cm$^2$, the forward voltage scanning range is −0.2 V to +1.4 V, the reverse voltage scanning range is +1.4 V to −0.2 V, and the size of the device is 0.0957 cm$^2$). The surface topography and conductivity test were performed using a CypherS atomic force microscope (AFM) produced by Oxford Instruments (Oxford, UK). The steady-state PL spectra and TRPL spectra were measured using FS5 (Edinburgh Instruments, Livingston, Scotland, UK), Laser wavelength: 365 nm. The impedance (EIS) test was performed on the device using an electrochemical workstation (ZAHNER-Elektrik GmbH, Dreieich, Germany), Instrument parameter Settings: (Frequency is 0.1 Hz–1 MHz, amplitude is 10 mV, bias voltage is 0.8 V). The open-circuit voltage $V_{OC}$ vs light intensity was measured using a carrier mobility measurement system (Fluxim, Paios 4.3, Winterthur, Switzerland). The space charge limited current (SCLC) was obtained by a 2400 Source Meter in a dark environment, under bias from 0.9 V to 1.5 V.

## RESULTS AND DISCUSSION

### Photovoltaic performance

To investigate the effect of Spiro-OMeTAD HTLs with varying oxidation times on PSC performance, PSCs featuring the architecture ITO/$SnO_2$/perovskite/Spiro-OMeTAD/Ag were fabricated, as depicted in Fig. 1(a). In this device, the perovskite layer absorbs incident light, while the $SnO_2$ and Spiro-OMeTAD layers serve as the electron transport layer (ETL) and HTL, respectively. Fig. 1(b) presents the current density-voltage ($J$-$V$) curves of PSCs using Spiro-OMeTAD as the HTL with different oxidation times. The key performance parameters of open-circuit voltage ($V_{OC}$), short-circuit current density ($J_{SC}$), fill factor (FF), and power conversion efficiency (PCE) are listed in Table 1. It can be observed that the performance of Spiro-OMeTAD-based devices gradually improves with increasing oxidation time, then declines after reaching the optimal duration of 96 h. The devices with the optimal oxidation time exhibit a best PCE of 16.69%, $V_{OC}$ of 1.14 V, $J_{SC}$ of 22.89 mA/cm$^2$, and FF of 67.69%. Fig. 2(b) and Table 1 show that devices treated with 96 h-oxidation achieve peak efficiency, while 24 h and 48 h treatments result in suboptimal performance due to incomplete oxidation. The 168 h group displays degradation characteristics associated with over-oxidation [32].

To validate the repeatability of photovoltaic performance parameters for devices fabricated under different oxidation time conditions, the parameters ($V_{OC}$, $J_{SC}$, FF, PCE) of 10 devices were analyzed, and the corresponding box plots are presented in Fig. 2. The device performance improved with increasing oxidation time up to the optimal duration. Peak performance was achieved at an oxidation time of 96 h, whereas the performance declined at an oxidation time of 168 h. The optimal 96 h-oxidation reduces carrier recombination rates, which enhances carrier transport properties [33] and results in improved the photoelectric conversion efficiency of devices [34].

### Changes in surface topography and conductivity

To investigate the impact of oxidation time on the morphology and conductivity of the Spiro-OMeTAD films, we used AFM in tapping and contact modes to characterize the morphological and conductivity changes of the Spiro-OMeTAD films with varying oxidation times, as presented in Fig. 3(a–h). The Spiro layer exhibited no obvious grain formation and remained in an incompletely oxidized state after 24 h of oxidation, as shown in Fig. 3(a,e). The morphology shows rudimentary

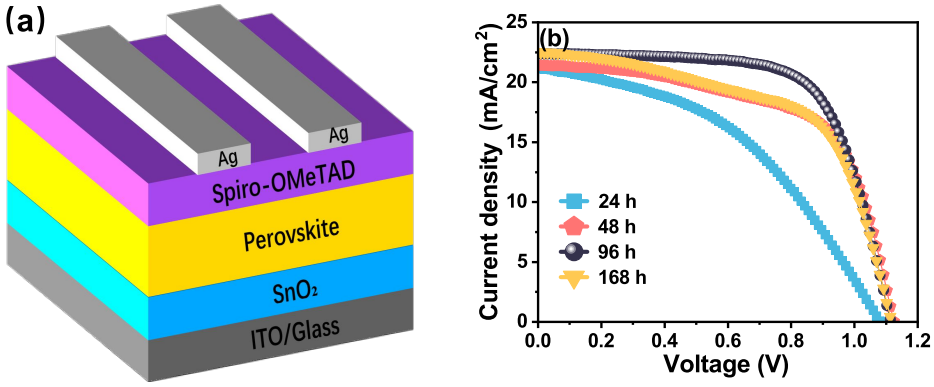


**Fig. 1** (a) Device structure of PSCs, (b) Photocurrent density-voltage curves of PSCs with Spiro-OMeTAD HTL for different oxidation times.

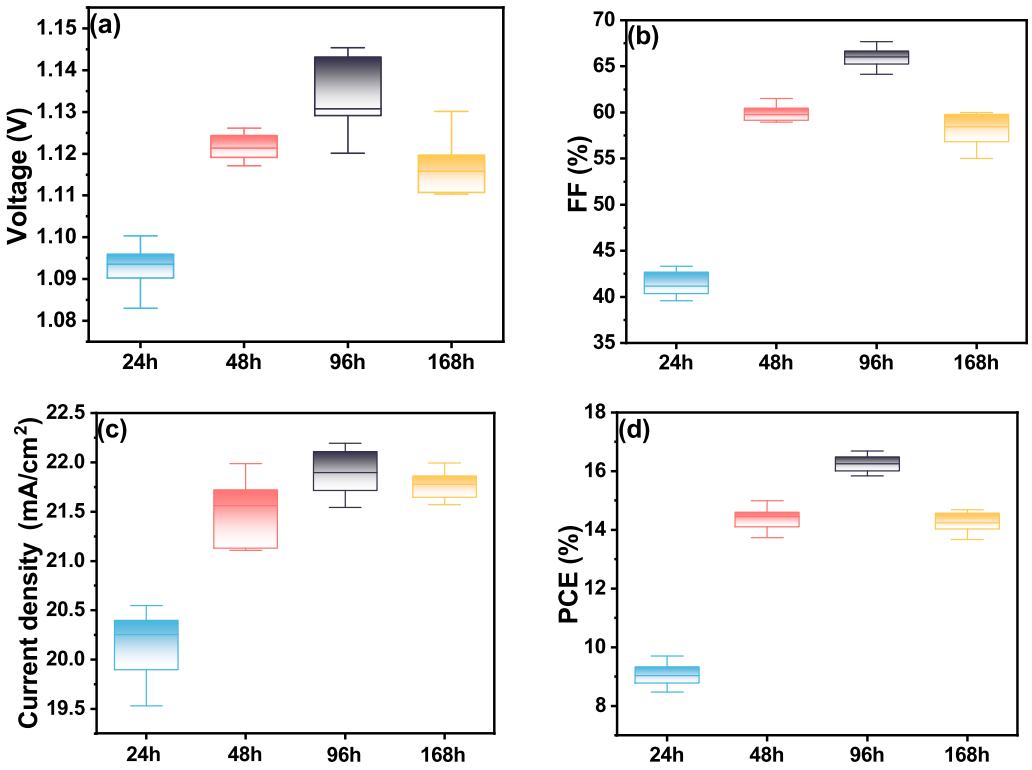


**Fig. 2** Box plots of photovoltaic parameters $V_{OC}$, $J_{SC}$, FF, and PCE of PSCs with Spiro-OMeTAD HTL for different oxidation time conditions.

**Table 1** Photovoltaic parameters of PSCs with Spiro-OMeTAD HTL for different oxidation time conditions.

| Time | | $V_{OC}$ (V) | $J_{SC}$ (mA/cm$^2$) | FF (%) | PCE (%) |
|---|---|---|---|---|---|
| 24 h | Average | 1.09 ± 0.01 | 20.14 ± 0.40 | 41.43 ± 3 | 9.06 ± 0.59 |
| | Best | 1.10 | 20.45 | 43.32 | 9.54 |
| 48 h | Average | 1.12 ± 0.02 | 21.45 ± 0.53 | 59.93 ± 2 | 14.38 ± 0.41 |
| | Best | 1.12 | 21.98 | 61.36 | 14.99 |
| 96 h | Average | 1.13 ± 0.02 | 21.89 ± 0.70 | 65.80 ± 2 | 16.25 ± 0.28 |
| | Best | 1.14 | 22.18 | 67.69 | 16.69 |
| 168 h | Average | 1.11 ± 0.02 | 21.76 ± 0.23 | 58.27 ± 2 | 14.23 ± 0.56 |
| | Best | 1.11 | 21.99 | 60.00 | 14.68 |

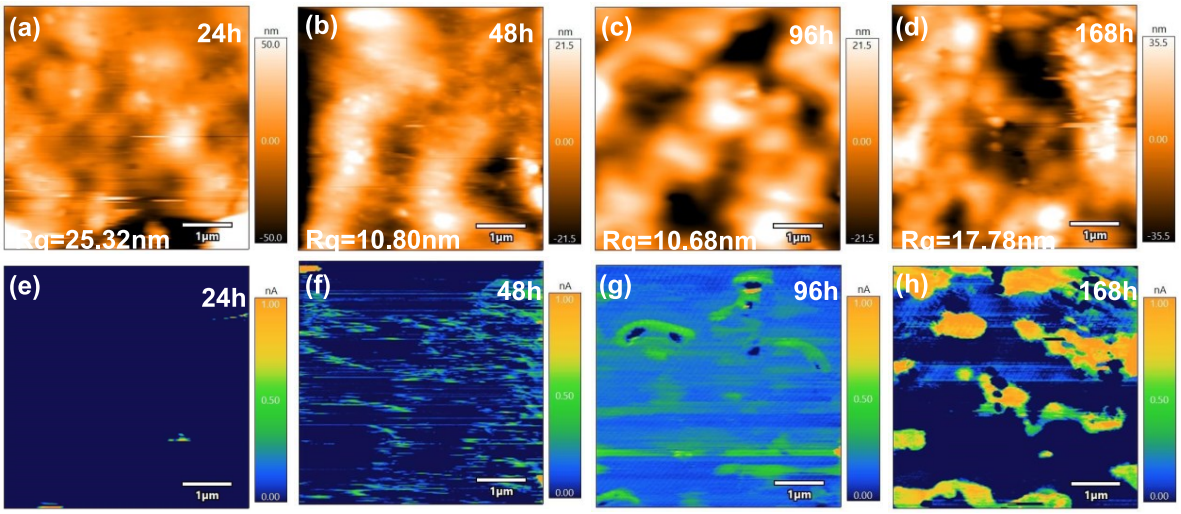


**Fig. 3** The AMF morphology images (a–d) and the surface potential distribution maps (e-h) of Li-TFSI and tBP-doped Spiro-OMeTAD films with different oxidation times.

grain shapes, but the crystals are not fully developed (Fig. 3(b,f)) for the film oxidized for 48 h. The 96 h-oxidized film shows distinct grain shapes with well-grown crystals and uniform distribution (Fig. 3(c,g)). The crystals of the 168 h-oxidized film started to degrade, with increased inter-grain spacing (Fig. 3(d,h)). The 96 h-oxidized sample with a root mean square roughness of 10.68 nm is smoother than the others, which probably enhances the carrier transport properties. The conductivity measurements indicated that the 24 h-oxidized Spiro-OMeTAD layer generated a negligible current. The 48 h-oxidized Spiro-OMeTAD layer surface began to produce current with extensive interfacial current generation. Compared to the 24 and 48 h-samples, the 96 h-oxidized Spiro-OMeTAD film exhibited a significantly higher surface potential with a wider distribution, which possibly enhances the electrical conductivity to improve the performance of PSCs. The surface potential of the samples with 168 h-oxidation slightly increased, but showed a narrower distribution, which caused the charge recombination in the devices [35].

## Spectral analysis

To further verify the effect of the oxidation time of the Spiro-OMeTAD layer on the device performance, we analyzed this effect using PL and time-resolved photoluminescence (TRPL) spectroscopy. The spectra of the Spiro-OMeTAD layer with different oxidation times exhibited distinct differences. The PL emission intensity of the 96 h-oxidized Spiro-OMeTAD film was significantly reduced (Fig. 4a), indicating that carrier extraction and transport were accelerated by the optimal oxidation time. This also implies that the 96 h-oxidized Spiro-OMeTAD layer minimizes non-radiative recombination and energy loss [36], thereby lowering the carrier recombination probability. Fig. 4(b) shows the TRPL spectra of Spiro-OMeTAD films with different oxidation times. The Spiro layer oxidized at the optimal 96 h duration showed the shortest carrier lifetime ($\tau_{avg}$ = 0.27 μs), whereas the 24 h, 48 h, and 168 h-samples exhibited longer lifetimes (0.63 μs, 0.48 μs, and 0.43 μs, respectively). This trend indicates an enhanced charge transfer efficiency in the Spiro-OMeTAD layer after 96 h of oxidation.

## Carrier transport

To further investigate carrier transport in PSCs with Spiro-OMeTAD films of different oxidation times, we characterized the $V_{OC}$ as a function of light intensity. Fig. 5(a) shows a monotonic increase in the $V_{OC}$ with light intensity. As is well known, the slope of the plot deviates from unity $kT/q$ (where $k$ is the Boltzmann constant, $T$ is the absolute temperature, and $q$ denotes the elementary charge) to induce trap-assisted recombination. Fig. 5(a) reveals pronounced trap-assisted recombination in the 24 h, 48 h, and 168 h-oxidized devices, leading to significant $V_{OC}$ losses. In contrast, 96 h-oxidation reduces recombination and defect density; the fitting line for the 96 h-device exhibits the smallest ideality factor ($n = 1.27kT/q$), consequently minimizing the voltage loss [37].

We measured the electrochemical impedance spectroscopy (EIS) of PSCs with Spiro-OMeTAD films for varying oxidation times, as shown in Fig. 5(b). The resulting Nyquist plots were aligned with experimental data. The charge transfer resistance ($R_{ct}$) of PSCs fabricated under optimal oxidation conditions was minimized, indicating that this condition reduces electron-hole recombination rates and effectively suppresses defect-mediated recombination [38]. Thus, PSCs with Spiro-OMeTAD films after the 96 h of oxidation demon-

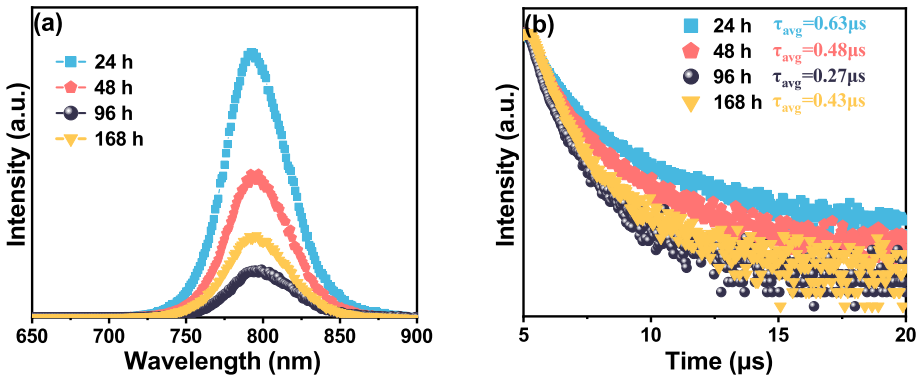


**Fig. 4** PL spectra (a) and TRPL spectra (b) of Li-TFSI and tBP-doped Spiro-OMeTAD films with different oxidation times.

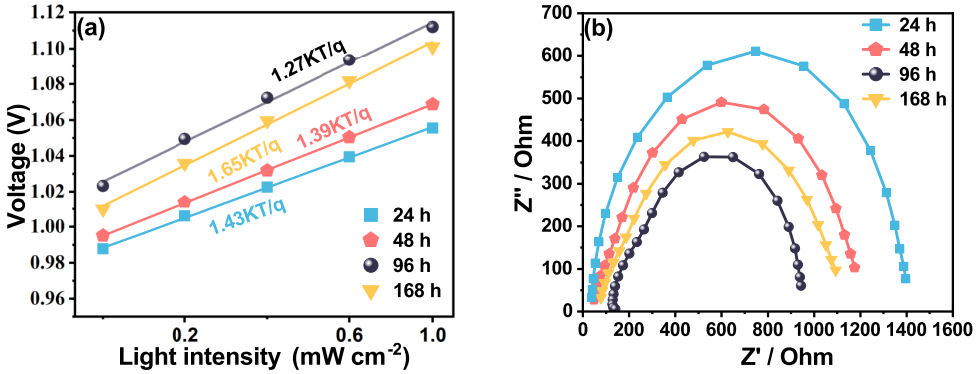


**Fig. 5** Plots of $V_{OC}$ versus light intensity (a) and Nyquist plots (b) of the PSC devices with Spiro-OMeTAD films for different oxidation times.

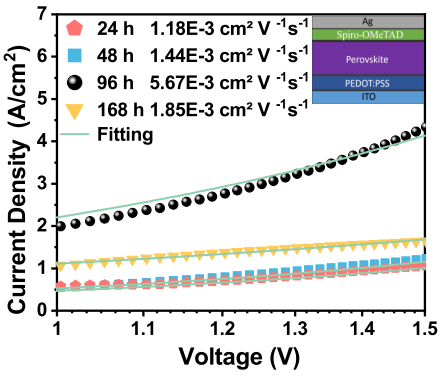


**Fig. 6** *J-V* curves of the hole-only device with structure of ITO/PEDOT:PSS/Perovskite/Spiro-OMeTAD under the dark condition.

strated superior photovoltaic performance. Furthermore, the acquired results exhibited good consistency with the AFM characterization.

In order to get more insight of influence of Spiro-OMeTAD with different oxidation times on charge mobility, we measured the *J-V* curves of the hole-only devices under the dark condition, as shown in Fig. 6. Mott-Gurney law equation is employed to calculated the hole mobility. The equation is illustrated as follows:

$$J = \frac{9}{8}\varepsilon\varepsilon_0\mu\frac{V^2}{L^3}$$

where $J$ = dark current density (mA/cm$^2$), $\varepsilon$ = relative permittivity of perovskite (dimensionless), $\varepsilon_0$ = permittivity of free space ($8.854 \times 10^{-14}$ F/cm). The equation applies to unipolar transport under dark space-charge-limited current (SCLC) conditions. The mobilities of Spiro-OMeTAD with different oxidation times are presented in Fig. 6. The mobility ($5.67\times10^{-3}$ cm$^2$/(V·s) of Spiro-OMeTAD oxidized for 96 h reached a maximum, indicating that the self-doping level and structural integrity of Spiro-OMeTAD have achieved an optimal balance-sufficient carrier concentration is attained without significant degradation. Beyond 96 h, the positive effect of self-doping became saturated, and excessive oxidation began to trigger adverse reactions.

## CONCLUSION

We fabricated PSCs with a Spiro-OMeTAD HTL for different oxidation times. Notably, control experiments further confirmed that oxidation times deviating from the optimal value led to compromised performance: insufficient oxidation ($\leqslant$ 48 h) resulted in incomplete crystallization of Spiro-OMeTAD and lower conductivity, exacerbating charge recombination; excessive oxidation ($geq$150 h) induced partial degradation of the Spiro-OMeTAD molecular structure, reducing its carrier mobility and disrupting the interfacial contact with the perovskite layer. At the optimal oxidation time, Spiro-OMeTAD forms a high-quality film with enhanced crystallization and carrier mobility, thereby improving the photovoltaic performance of PSCs. Specifically, PSCs with a Spiro-OMeTAD HTL at the optimal oxidation time achieved a maximum PCE of 16.69%. This study underscores the importance of precise oxidation time control in tailoring the properties of Spiro-OMeTAD HTMs and provides a facile, low-cost strategy for improving the efficiency and reproducibility of PSCs, offering valuable insights for the rational design of HTM post-processing protocols in perovskite photovoltaic technology.

*Acknowledgements*: This research was supported by the Natural Science Foundation of Inner Mongolia Autonomous Region (2023LHMS06015 and 2019MS02015), the Higher Education Scientific Research Projects of Inner Mongolia (NJZY21568), the Fundamental Research Funds for Inner Mongolia Normal University (2022JBQN083).

## REFERENCES

1. Cheng X, Yang S, Cao B, Tao X, Chen Z (2019) Single crystal perovskite solar cells: Development and perspectives. *Adv Funct Mater* **30**, 1905021.
2. Jeong J, Kim M, Seo J, Lu H, Ahlawat P, Mishra A, Yang Y, Hope MA, et al (2021) Pseudo-halide anion engineering for α-$FAPbI_3$ perovskite solar cells. *Nature* **592**, 381–385.
3. Xiao K, Lin R, Han Q, Hou Y, Qin Z, Nguyen HT, Wen J, Wei M, et al (2020) All-perovskite tandem solar cells with 24.2% certified efficiency and area over 1 $cm^2$ using surface-anchoring zwitterionic antioxidant. *Nat Energy* **5**, 870–880.
4. Ng A, Ren Z, Hu H, Fong PWK, Shen Q, Cheung SH, Qin P, Lee J, et al (2018) Perovskite solar cells: A cryogenic process for antisolvent-free high-performance perovskite solar cells. *Adv Mater* **30**, 1870329.
5. Al-Ashouri A, Köhnen E, Li B, Magomedov A, Hempel H, Caprioglio P, Márquez JA, Vilches ABM, et al (2020) Monolithic perovskite/silicon tandem solar cell with > 29% efficiency by enhanced hole extraction. *Science* **370**, 1300–1309.
6. Shen H, Walter D, Wu Y, Fong KC, Jacobs DA, Duong, Peng J, Weber K, et al (2019) Monolithic perovskite/SI tandem solar cells: Pathways to over 30% efficiency. *Adv Energy Mater* **10**, 1902840.
7. Kim JY, Lee J-W, Jung HS, Shin H, Park N-G (2020) High-efficiency perovskite solar cells. *Chem Rev* **120**, 7867–7918.
8. Kojima A, Teshima K, Shirai Y, Miyasaka T (2009) Organometal halide perovskites as visible-light sensitizers for photovoltaic cells. *J Am Chem Soc* **131**, 6050–6051.
9. Min H, Lee DY, Kim J, Kim G, Lee KS, Kim J, Paik MJ, Kim YK, et al (2021) Perovskite solar cells with atomically coherent interlayers on $SnO_2$ electrodes. *Nature* **598**, 444–450.
10. Zhang T, Long M, Qin M, Lu X, Chen S, Xie F, Gong L, Chen J, et al (2018) Stable and efficient 3D-2D perovskite-perovskite planar heterojunction solar cell without organic hole transport layer. *Joule* **2**, 2706–2721.
11. Byranvand MM, Saliba M (2021) Charge carrier management for developing high-efficiency perovskite solar cells. *Matter* **4**, 1758–1759.
12. Chen Z, Wang Y, Shen H (2025) Enhancing absorption efficiency by incorporating hollow titanium particles in perovskite solar cells. *ScienceAsia* **51**, ID 2025055.
13. Kim Y, Jung EH, Kim G, Kim D, Kim BJ, Seo J (2018) Sequentially fluorinated PTAA polymers for enhancing $V_{OC}$ of high-performance perovskite solar cells. *Adv Energy Mater* **8**, 1801668.
14. Volkov AV, Wijeratne K, Mitraka E, Ail U, Zhao D, Tybrandt K, Andreasen JW, Berggren M, et al (2017) Understanding the capacitance of PEDOT:PSS. *Adv Funct Mater* **27**, 1700329.
15. Zhou J, Tan L, Liu Y, Li H, Liu X, Li M, Wang S, Zhang Y, et al (2024) Highly efficient and stable perovskite solar cells via a multifunctional hole transporting material. *Joule* **8**, 1691–1706.
16. Manit J, Kanjanaboos P, Naweephattana P, Naikaew A, Srathongsian L, Seriwattanachai C, Supruangnet R, Nakajima H, et al (2024) Towards device stability of perovskite solar cells through low-cost alkyl-terminated SFX-based hole transporting materials and carbon electrodes. *Sci Rep* **14**, 24167.
17. Ouedraogo NAN, Odunmbaku GO, Guo B, Chen S, Lin X, Shumilova T, Sun K (2022) Oxidation of Spiro-OMETAD in high-efficiency perovskite solar cells. *ACS Appl Mater Interfaces* **14**, 34303–34327.
18. Gao S, Li X, Cao R, Li X, Chen T, Lu Y, Zhu J, Yang S (2024) Hot pure oxygen accelerated oxidation of Spiro-OMeTAD for efficient perovskite solar cells with a record certified fill factor exceeding 87%. *ACS Energy Lett* **9**, 5037–5044.
19. Chen Q, Wu J, Wang X, Li G, Song Z, Xu Y, Deng C, Du Weihai Sun Y, Lan Z (2022) 3-Chloroperoxybenzoic acid doping spiro-OMeTAD for improving the performance of perovskite solar cells. *Chem Eng J* **450**, 138313.
20. Szabó G, Kamat PV (2024) Spiro-OMETAD: Unique redox chemistry driving the hole transport. *ACS Energy Lett* **10**, 330–336.
21. Xue J, Wang R, Chen X, Yao C, Jin X, Wang K-L, Huang W, Huang T, et al (2021) Reconfiguring the band-edge states of photovoltaic perovskites by conjugated organic cations. *Science* **371**, 636–640.
22. Chang Q, Yun Y, Cao K, Yao W, Huang X, He P, Shen Y, Zhao Z, et al (2024) Highly efficient and stable perovskite solar modules based on FCPF6 engineered

Spiro-OMETAD hole transporting layer. *Adv Mater* **36**, 2406296.

23. He D, Ma D, Li R, Liu B, Zhou Q, Yang H, Lu S, Zhang Z, et al (2024) Synergistically stabilizing hole transport layer and dual interface enables high-performance perovskite solar cells. *ACS Energy Lett* **9**, 2615–2625.
24. Correa-Baena J-P, Saliba M, Buonassisi T, Grätzel M, Abate A, Tress W, Hagfeldt A (2017) Promises and challenges of perovskite solar cells. *Science* **358**, 739–744.
25. Ding C, Huang R, Ahläng C, Lin J, Zhang L, Zhang D, Luo Q, Li F, et al (2021) Synergetic effects of electrochemical oxidation of Spiro-OMeTAD and $Li^+$ ion migration for improving the performance of n-i-p type perovskite solar cells. *J Mater Chem A* **9**, 7575–7585.
26. Wang S, Huang Z, Wang X, Li Y, Günther M, Valenzuela S, Parikh P, Cabreros A, et al (2018) Unveiling the role of TBP-LITFSI complexes in perovskite solar cells. *J Am Chem Soc* **140**, 16720–16730.
27. Cao F, Zhu Z, Zhang C, Chen P, Wang S, Tong A, He R, Wang Y, et al (2023) Synergistic ionic liquid in hole transport layers for highly stable and efficient perovskite solar cells. *Small* **19**, 2207784.
28. Pan T, Li Z, Ren B, Yang W, Ran X, Li Y, Xu Y, Wang Y, et al (2024) Stabilizing doped Spiro-OMeTAD with an organic molten salt for efficient and stable perovskite solar cells. *Energy Environ Sci* **17**, 9548–9554.
29. Hawash Z, Ono LK, Raga SR, Lee MV, Qi Y (2022) Correction to air-exposure induced dopant redistribution and energy level shifts in spin-coated Spiro-MeOTAD films. *Chem Mater* **34**, 3882.
30. Ono LK, Schulz P, Endres JJ, Nikiforov GO, Kato Y, Kahn A, Qi Y (2014) Air-exposure-induced gas-molecule incorporation into Spiro-MeOTAD films. *J Phys Chem Lett* **5**, 1374–1379.
31. Shin YS, Lee J, Sung MJ, Jeon I, Jeon NJ, Kim DS (2025) Intrinsic and extrinsic determinants of stability in Spiro-OMETAD-based hole-transporting layers in perovskite solar cells: Mechanistic insights and strategic perspectives. *Adv Mater* **37**, 13270.
32. Chen Q, Wu J, Wang X, Yang Y, Du Y, Li Z, Zhang X, Zhang Z, et al (2021) Spiro-OMeTAD doped with cumene hydroperoxide for perovskite solar cells. *Electrochem Commun* **126**, 107020.
33. Liu X, Zheng B, Shi L, Zhou S, Xu J, Liu Z, Yun JS, Choi E, et al (2023) Perovskite solar cells based on spiro-OMeTAD stabilized with an alkylthiol additive. *Nat Photonics* **17**, 96–105.
34. Liu M, Wang Y, Lu C, Zhu C, Liu Z, Zhang J, Yuan M, Feng Y, et al (2024) Localized oxidation embellishing strategy enables high-performance perovskite solar cells. *Angewandte Chemie Int Edn* **63**, e202318621.
35. Yoo JJ, Seo G, Chua MR, Park TG, Lu Y, Rotermund F, Kim Y-K, Moon CS, et al (2021) Efficient perovskite solar cells via improved carrier management. *Nature* **590**, 587–593.
36. Yang J, Xiong S, Song J, Wu H, Zeng Y, Lu L, Shen K, Hao T, et al (2020) Energetics and energy loss in 2D ruddlesden-popper perovskite solar cells. *Adv Energy Mater* **10**, 2000687.
37. Ren X, Wang ZS, Choy WCH (2019) Device physics of the carrier transporting layer in planar perovskite solar cells. *Adv Opt Mater* **7**, 1900407.
38. Ye Y, Chen L, Chen X, Ma C, Lv B, Wang J, Dou W, Zhang C, et al (2023) Interfacial energy level alignment and defect passivation by using a multifunctional molecular for efficient and stable perovskite solar cells. *Adv Funct Mater* **34**, 2310136.